Journal of Innovation and Development
ISSN: 2958-4752 | Vol. 2, No. 3, 2023

Experimental and numerical studies of low power Hall thruster performance

Xiaoxian Wang [1, a], Zongqi Xu [2], Pingyang Wang [2], Yajun Huang [1], Guomin Cui [1, *]

[1] School of Energy and Power Engineering, University of Shanghai for Science and Technology, Shanghai, China
[2] School of mechanical and power engineering, Shanghai Jiao tong university, Shanghai, China

[*] **Corresponding author**: Guomin Cui (Email: cgm@usst.edu.cn), [a]18550219351@163.com

Abstract: The low power Hall thruster has the potential to be applied in multiple apace missions. In order to study the performance of the low power Hall thruster, a 200W-class Hall thruster is designed and manufactured. The plasma properties in the discharge channel are investigated via numerical simulation. The ionic composition and ion current density are respectively measured by a Wien filter and a Faraday probe. The generated thrust is measured by a thrust target. The simulation results show that the maximal ion number density is more than 1×1018 m-3. The ionization and acceleration regions are located in the midstream and downstream of the discharge channel. The experimental results reveal that thrust, anode specific impulse and anode efficiency are 12.13 mN, 1380 s, and 41% at 200 W. The ion current density decreases along the radial direction. According to the results of simulation and experiment, the thruster is reasonable and feasible. Our research provides a reference for the design of low power Hall thruster. Structural optimization and performance improvement will be carried out further.

Keywords: Electric propulsion; Low power Hall thruster; Plasma property; Plasma diagnostic; Thrust measurement.

1. Introduction

Hall-effect thruster, with the characteristics of high specific impulse and thrust density, is a promising electric propulsion device in space. They are suitable for multiple space missions as a dynamical system including station keeping and orbit transferring. Along with the development of the micro and small satellites, there is a demand for the miniaturization of the thruster for advanced missions. Therefore, the low-power Hall thrusters have attracted much attention, especially in the commercial satellite field. Busek Co. Inc focused on the low-power Hall thruster research for decades and the BHT-200 became the first American HET to fly in space as part of the U.S. Air Force TacSat-2 satellite in 2006 [1]. Holak Kim et al. studied the plume characteristics of a 50-100 W cylindrical Hall thruster measured and analyzed by a Faraday probe and a retarding potential analyzer [2]. Tomoyuki Ikeda et al. designed a series of low-power cylindrical type Hall thrusters for Nano Satellites and acquired the specific impulse, the thrust and the thrust efficiency [3-5]. Found in their test, one of the thrusters could stably operate even with 10 W [6]. Jason D Frieman et al. tested the Aerojet Rochetdyne T-40 low-power Hall with both xenon and krypton. The thrust of the krypton-operated is lower than that of the xenon-operated, but the anode specific and anode efficiency are opposite [7]. Smirnov A found that the cylindrical Hall thruster suffered lower erosion of the channel walls compared with the conventional annular Hall thruster, because of its lower surface-to volume [8]. Ryan W. Conversano et al. improved the thruster performance through the optimization of the magnetic field [9]. Garrigues L et al. used a hybrid PIC/fluid approach to simulate two different magnetic fields in order to investigate the impact of erosion on channel walls [10]. The ion velocity distribution is also affected by the background pressure in low-power Hall thruster [11]. Matthew Baird et al. obtained a quiescent sinusoidal discharge current in only the low flow and voltage operation condition [12]. Duan X Y et al. investigated the far-field plasma characterization in a 600W Hall thruster [13]. Ding Y J et al. found the point of intersection of the characteristic magnetic field line with the channel wall affected the performance and lifetime of the low power cylindrical Hall thruster [14]. In a word, many research institutions have been studying the discharge characteristics of the low power Hall thrusters. This paper deals with a xenon-fueled 200 W-class Hall thruster designed by our lab. First, the thruster structure and magnetic field configuration are described. Second, thrust and plasma performance levels are given and compared under different operation parameters. Finally, the plasma physical property parameters are reported.

2. Magnetic field characteristics

The ignition of Hall thruster cannot realize without crossed electric and magnetic fields to generate and accelerate ions [15]. The radial magnetic field inhibits electrons from traveling from cathode to anode. The result of a large number of electrons gathering at the channel exit with a Larmor gyratory motion is that an axial electric field is generated inside the discharge channel by which the ions are accelerated outward. Therefore, the magnetic field configuration almost completely determines the positions of the ionization and acceleration regions which have an important impact on the thruster performance. In order to make the maximum of the magnetic field appear near the channel exit and keep the magnetic flux density almost zero near the anode area, the magnetic shielding configuration is employed as illustrated in Figure 1.

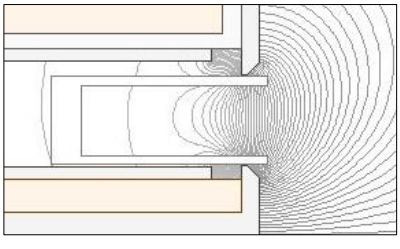

Figure 1. Magnetic field distribution near the channel exit.

In addition, the configuration is conductive to reduce the wall erosion caused by the ion bombardment. In this paper, the experimental and computational results both base on our designed low power Hall thruster with a magnetically shielded configuration.

3. Experimental setup

3.1. Thruster and vacuum facility

The thruster, shown in Figure 2, operated at about 200 W power level. Table 1 shows the operating conditions of the thruster in the test. The depth of the annular channel is 20 mm and the outer and the inner diameters of it are 50 mm and 26.75 mm, respectively. The overall length and diameter of the thruster are both about 90 mm. The magnetic circuit consists of two copper coils connected to different channels of the power supply. The magnitude and topology of the magnetic field near the discharge channel exit are able to change by the adjustment of the currents in the coils. The discharge channel, made of boron nitride, has two apertures located in the upstream which are designed for propellant and power inlets. The axial direction gas supply distribution, made of 316 stainless steel, is placed in the upstream of the discharge channel as the anode, and Figure 3 is the sectional drawing. The electron source used to form a virtual cathode in the discharge channel exit plane and neutralize the ions in the plume is a hollow cathode with lanthanum hexaboride (LaB6) emitter.

Figure 2. Image of the low power Hall thruster.

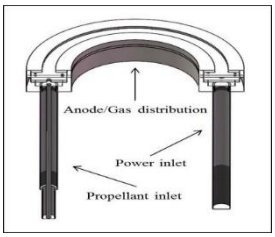

Figure 3. Sectional drawing of gas supply distribution.

Table 1. Operating conditions of the Hall thruster.

Parameters	Anode Flow	Cathode Flow	Discharge voltage	Discharge Current	Magnet Current	Heater Current	Keeper Current
Value	897μg/s	135μg/s	200V	1.0A	0.7A	4.0A	1.0A

Experimental testing was conducted in a high vacuum electric propulsion test platform. The facility refers to a cylindrical carbon-steel vacuum chamber measuring 1.5 m in diameter and 3 m long. The chamber is equipped with three vane rotary pumps, one roots pump and two oil diffusion pumps. The vane rotary pump and the roots pump as the fore pumps have the pumping speeds of 80 L/s and 600 L/s. The oil diffusion pumps with a total pumping speed of 33000 L/s play a major role in the vacuum performance of the chamber. The chamber pressure is monitored by a resistance gauge and an ionization gauge for low vacuum degree and high vacuum degree. The base pressure of this system is less than 2×10-4 Pa under the conditions of the whole pumps operations and the pressure was sustained below 5.6×10-2 Pa under a total Xe flow of 10 sccm. Plume and beam properties were measured by a Wien filter and a Faraday probe. The experiment was carried out under a 6-8 sccm Xe flow rate for anode and a 2-3 sccm Xe flow rate for cathode. The thruster was stably operated under an anode voltage of 200-250 V. The operating state was depicted in Figure 4, which was operated as the parameters in Table 1.

Figure 4. Low power Hall thruster operation with Xe at 200W-class

3.2. Thrust measurement

For an electric thruster, thrust is an important parameter to evaluate whether to satisfy the different space missions. Also, specific impulse and thrust efficiency are able to acquire further. The thrust was measured in our experiments by a 550 mm aluminous circular thrust target, which was placed at a distance of 350 mm from the discharge channel exit plane, and coaxial with the vacuum chamber, as shown in Figure 5. The target mass was about 300 g. The thrust measurement device consisted of a suspended target, a displacement sensor and several aluminum profiles. The target was fixed to the aluminum profiles by two light ropes. The sensor, installed at a distance of about 20 mm from the center of the target, had the capable of obtaining the target's horizontal displacement value caused by the exhaust ions. The thrust can be described as

$$T = \frac{Xm_0 g}{\sqrt{L^2 - X^2}} \quad (1)$$

Here X is the kinetic distance of the target, m0 is the target mass, g is the acceleration of gravity, L is the distance from the top of the torsional wire to the center of the target.

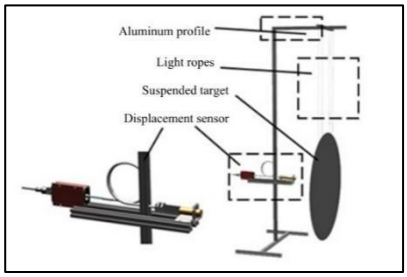

Figure 5. Schematic of the thrust measurement system

4. Plasma diagnostics

In order to analyze the plasma performance in the plume, a Wien filter and a Faraday probe are designed and utilized for the measurement of current density and ion composition.

4.1. Wien filter

Wien filter, also called E×B probe, is a passband velocity filter for charged particles. It separates different ions in the plume based on the Lorentz force. Kim used a Wien filter to measure the ion energy distribution in the plume of a SPT-100 in 1999, which becomes the first attempt to apply it in the Hall-effect thruster diagnostic. Other studies about the Wien filter included the ion species fraction analysis and multi-angular measurement.

The Wien filter designed and used in our experiment consists of four sections: a collimator, an E×B stage, a drift region, and a collector, as shown in Figure 6. The collimator, made of the 316 stainless steel, is grounded with a 1mm orifice to minimize the acceptance angle of the probe, which is within ±0.5 degrees. The length in the collimator satisfied the angle. The collector is made of tungsten to reduce secondary emissions. The ions with a velocity vector that was not parallel to the axis of the Wien filter in the exhaust would be filtered out when travelling in the collimator and drift region. In the E×B stage, an electric field E, existed between the plates, is perpendicular to a magnetic flux density B. The charged particles via the collimator would travel along the direction perpendicular to E and B, and were subjected to an electric field force and a Lorentz force in the opposite direction. The total force is described as

$$F = qe\left(\vec{E} + \vec{u} \times \vec{B}\right) \tag{2}$$

Here e is the elementary charge, and q is the ion charge number. Only the particles with a unique velocity could pass though this section without any trajectory deviation under a certain electric field. The velocity is defined as

$$u = \frac{E}{B} = \frac{U}{Bd} \tag{3}$$

Here U is the applied potential, and d is the distance between two parallel plates. The velocity of ions in the exhaust is given by Goebel and Katz

$$u = \sqrt{\frac{2qeV_d}{m}} \tag{4}$$

Here Vd is the acceleration voltage, and m is the ion mass. The travelling ions with a velocity v are eventually captured and neutralized by the collector. The ionic current is measured by a Keithley 6487 Pico ammeter. For a Wien filter, the structure is fixed, including the size of the plates and distance between the plates. The magnetic flux density is determined by the Samarium Cobalt permanent magnet, whereas the electric potential of the plates is controlled by a power supply. The ion velocity resolution of the filter Δv, linked to the geometry of the filter, to the mass and charge of the ion species, and to the velocity u, must satisfy the following conditions

$$\Delta v \le \frac{m v_z^{\,2}}{qeB}\left[\frac{2\left(L_2 + L_3 + L_4\right)D_2 + \left(D_3 + D_2\right)L_1}{\left(L_3^{\,2} + 2L_3L_4\right)L_1}\right] \tag{5}$$

$$\Delta v \le \frac{m v_z^{\,2}}{qeB}\left[\frac{2\left(L_2 + L_3 + L_4 + L_5\right)D_2 + \left(D_C + D_2\right)L_1}{\left(L_3^{\,2} + 2L_3L_4 + 2L_3L_5\right)L_1}\right] \tag{6}$$

Here, vz is the axial velocity of the travelling ions, and |vz|≈|u|. D1, D2 are the orifice diameters at the entrance and exit of the collimator respectively, and D1=D2; D3 is the diameter of the drift tube; L1 is the collimator length; L2 is the distance between the collimator and the E×B stage; L3 is the length of the E×B fields region; L4 is the distance between the drift tube and the E×B stage; L5 is the length of the drift tube; DC is the diameter of the collector.

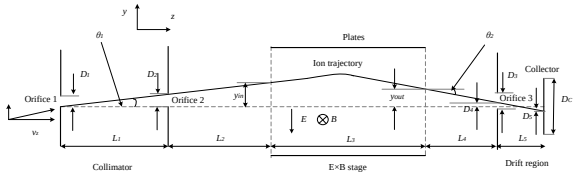

Figure 6. Schematic of the Wien filter, including the collimator, the E×B stage, the drift tube and the collector

4.2. Faraday probe

A Faraday probe is the common instrument used in the plume to measure the ion current density. The probe mainly consists of a collector plate and a guard ring, shown as Figure 7.

Figure 7. Nude Faraday probe.

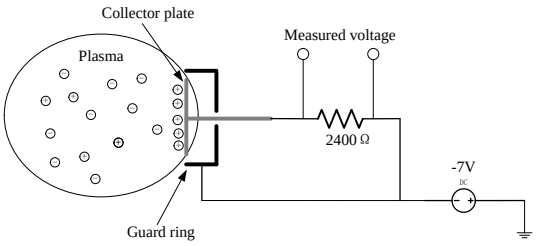

Figure 8. Schematic of Faraday probe circuit.

Both of them are biased negatively to 7 V to repel electrons and ensure a uniform potential field. The diameter of the collector plate is 10mm. The guard ring, around it with a 0.2 mm gap, has a function of attracting low energy ions from the sides of the probe which may cause an error in the ion current density measurement. After a biased voltage is applied to the collector plate and the guard ring, only ions are able to move towards the flat plate to induce a current. The current is affected by some factors, including the material of the plate, the ionic species in the plume and so on. The ions will be neutralized by the electrons supplied by the probe circuit. Therefore, it could be considered that the ion current is equal to current in the circuit. Nevertheless, almost every material would emit secondary electrons when colliding with high energy ions which results in higher measurements than actual. For a reduction of secondary electron emission, the collector

plate was made of tungsten. In our experiments, the effect on ion current measurement caused by secondary emission was negligible.

The current density was not acquired from the collector plate directly but a voltage across a resistor in the probe circuit. It could be expressed as

$$j = \frac{V}{R \cdot A} \tag{7}$$

Here V is the measured voltage; R is the resistance in the probe circuit; A is the area of the collector plate. Then, ion current in the plume could be estimated through the current density. A diagram of Faraday probe circuit is illustrated as Figure 8. In addition, there were two assumptions in the probe data collection and processing. First, the plume was assumed to be symmetric about the central axis of the thruster. Second, the whole current was moving towards the back of the tank. Based on the above assumptions, the ion current in the plume could be acquired by an integral of a half-spherical shell of current densities.

$$I = 2\pi r^2 \int_0^{\pi/2} j(\theta)\sin(\theta)d\theta \tag{8}$$

The integral value was estimated numerically with a rectangular method.

5. Experimental results and analysis

5.1. Thrust performance

Thrust (T) is used for the thruster performance assessment, based on which other macroscopic performance parameters could be calculated and obtained, including the anode specific impulse (Isp) and the anode efficiency (ηa). They are defined as

$$I_{sp} = \frac{T}{\dot{m}_a g} \tag{9}$$

Here $\dot{m}_a$ is the anode mass flow rate.

$$\eta_a = \frac{T^2}{2\dot{m}_a U_d I_d} \tag{10}$$

Here Ud and Id are the discharge voltage and the discharge current.

The thrust was measured by the thrust target. A horizontal displacement of about 3.3mm was existed after the thruster operated in a stable ignition state. From the above equations (1), (9), (10), the calculated results of the thrust and the anode specific impulse were about 12.13 mN and 1380 s respectively, and meanwhile the anode efficiency was about 41.0081%.

5.2. Plume characteristics

Except the thrust measurement, the plasma properties in the plume considered as an evaluation criterion to determine a thruster performance. Faraday probe was employed to measure the spatial distribution of the ion current density. Figure 9 represents the Faraday date of different angles in the plume at 200 W discharge power. The angle off centerline varied from 0 to 90 degrees at intervals of 10 degrees. Because of the finite measurement points, the equation (8) was simplified as

$$I = 2\pi r^2 \left(j(0)\sin(\frac{\pi}{36})\cdot\frac{\pi}{36} + \sum_{i=1}^{8} j(\frac{n\pi}{18})\sin(\frac{n\pi}{18})\cdot\frac{\pi}{18} + j(\frac{\pi}{2})\sin(\frac{\pi}{2})\cdot\frac{\pi}{36} \right) \tag{11}$$

Here, r was the distance between the discharge channel exit plane and collector plate of Faraday probe, and R=250 mm. As a consequence, the ion current was approximately 0.774 A.

The ion mass flow rate could be estimated through Faraday probe. The ion species and currents measured by Wien filter along with Faraday data were helpful for efficiency calculation. Figure10 presents the result of Wien filter measurement at 200 W. The angle off centerline varied from 0 to 20 degrees at intervals of 10 degrees.

In order to analyze the ionic physical properties in the plume, the parameters acquired by Wien filter raw data was fitted with Levenberg-Marquardt method and the fitted results were given in Figure 11.

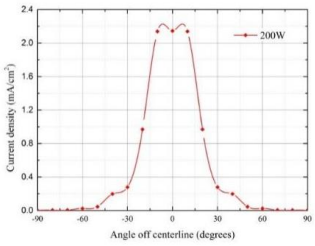

Figure 9. Ion current density distribution measured by Faraday probe

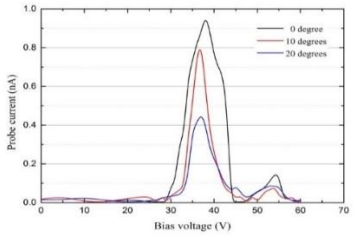

Figure 10. Raw data of probe current measured by Wien filter at 200 W.

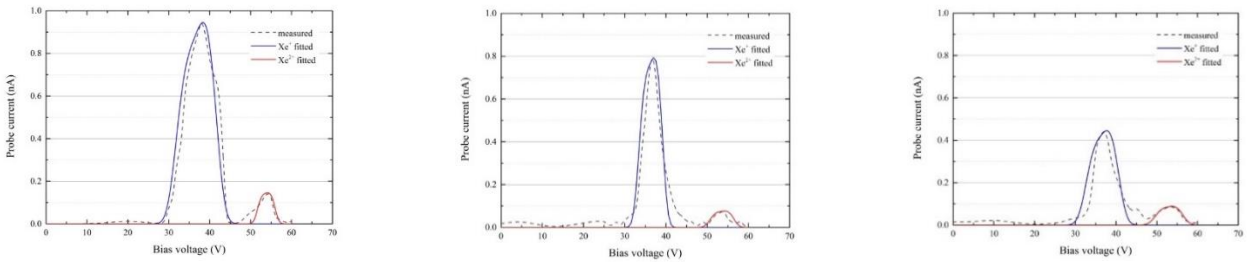

(a) (b) (c)

Figure 11. Wien filter raw data at 200W, (a) 0 degree, (b) 10 degrees, (c) 20 degrees.

The Faraday probe data provided the information of ion current in the plume, and that the other terms in the anode

efficiency calculation could be acquired by combining with the Wien filter data.

5.3. Current utilization efficiency

Because multiple ions exist in the plume, the number density of the ion beam is expressed as

$$n_b = \sum_{i=1}^{N} n_i \tag{12}$$

Here i is the number ion species, and the corresponding number proportion is

$$\xi_i = \frac{n_i}{n_b} \tag{13}$$

The formed current is

$$I_i = n_i u_i q_i S = n_i e Z_i S \sqrt{\frac{2eZ_i V_a}{m}} \cos\theta = n_b e^{3/2} S \sqrt{\frac{2V_a}{m}} \xi_i Z_i^{3/2} \cos\theta \tag{14}$$

Here Va is the effective acceleration voltage; S is beam cross section area; θ is the angle between the ion velocity direction and the symmetric axis. The total beam current is

$$I_b = \sum I_i = n_b e^{3/2} S \sqrt{\frac{2V_a}{m}} \cos\theta \sum \xi_i Z_i^{3/2} \tag{15}$$

The corresponding current proportion is

$$\Omega_i = \frac{I_i}{I_b} = \frac{\xi_i Z_i^{3/2}}{\sum \xi_i Z_i^{3/2}} \tag{16}$$

The current utilization efficiency is

$$\eta_b = \frac{I_b}{I_d} \tag{17}$$

Here I_d is the discharge current.

5.3.1. Mass utilization efficiency

The mass flow of the different ions is expressed as

$$\dot{m}_i = \frac{m}{e}\frac{I_i}{Z_i} = \frac{mI_b}{e}\frac{\Omega_i}{Z_i} \tag{18}$$

Therefore, the total mass flow is

$$\dot{m}_b = \sum m_i = \frac{mI_b}{e} \sum \frac{\Omega_i}{Z_i} \tag{19}$$

The mass utilization efficiency is

$$\eta_m = \frac{\dot{m}_b}{\dot{m}_a} = \frac{mI_d \eta_b}{\dot{m}_a e} \sum \frac{\Omega_i}{Z_i} \tag{20}$$

Here $\dot{m}_b$ is the mass flow of ionized particles and $\dot{m}_a$ is the mass flow of the whole particles.

5.3.2. Voltage utilization efficiency

The axial component of the ion velocity is

$$\langle u_i \rangle = \sqrt{\frac{2eV_a}{m}} \sqrt{Z_i} \cos\theta \tag{21}$$

The voltage utilization efficiency is

$$\eta_V = \frac{V_a}{V_d} \tag{22}$$

Here V_d is the discharge current

5.3.3. Plume divergence utilization efficiency

Because only axial component of the ion velocity contributes to the thrust, the charge-weighted divergence angle of the whole ions can be expressed as

$$\cos\beta = \frac{2\pi r^2 \int_0^{\pi/2} j(\theta)\cos\theta \sin\theta d\theta}{2\pi r^2 \int_0^{\pi/2} j(\theta)\sin\theta d\theta} \tag{23}$$

The plume divergence utilization efficiency is

$$\eta_d = (\cos\beta)^2 \tag{24}$$

5.3.4. Charge utilization efficiency

The thrust generated by the entire ions is

$$T = \sum \dot{m}_i u_i = \eta_b I_d \sqrt{\frac{2m\eta_V V_d}{e}} \sum \frac{\Omega_i}{\sqrt{Z_i}} \cos\theta \tag{25}$$

From the above equations (17), (20), (22) and (24), the corresponding anode efficiency is

$$\eta_a = \frac{T^2}{2\dot{m}_a P_d} = \eta_b \eta_V \eta_m \eta_d \frac{\left(\sum \Omega_i / \sqrt{Z_i}\right)^2}{\sum \Omega_i / Z_i} \tag{26}$$

The charge utilization efficiency is

$$\eta_q = \frac{\left(\sum \Omega_i / \sqrt{Z_i}\right)^2}{\sum \Omega_i / Z_i} \tag{27}$$

Eventually, the anode efficiency is written as

$$\eta_a = \eta_b \eta_V \eta_m \eta_d \eta_q \tag{28}$$

Plume data closely agrees with performance date on efficiency. According to the calculated results, the anode efficiency from the plume data was slightly higher than that from the performance date. This illustrated the Wien filter was off design point of low power Hall thruster, and this efficiency would decrease after an optimized design. Table 2 shows the whole efficiencies that were calculated on the basis of plume measurements and makes a comparison of the total anode efficiency of plume measurement and performance measurement.

Table 2. Measured efficiencies in the plume.

Parameter	η_b	η_V	η_m	η_d	η_q	η_a (plume)	η_a (performance)
Value	77.3%	86.6%	82.9%	82.2%	99.1%	45.2%	41.0%

6. Computational results and analysis

6.1. Simulated model

PIC/MCC (Particle in cell/ Monte Carlo collision) simulation is a common method of plasma parameters analysis. In this paper, it was used in conjunction with DSMC (Direct simulation Monte-Carlo) method. The PIC/MCC method is able to simulate the neutral gas, electrons and ions, obtaining the information of position, speed and energy. The DSMC method solves the coupled equations of motion and collision. The Maxwell distribution provides the initial speed

of the new particles, and the Poisson equation is solved by five-point difference method. The simplified model of the Hall thruster is shown in Figure 12. The length of the simulated channel is 20 mm. In the discharge channel, the left lateral boundary is the anode, while both the lower and upper boundaries are dielectric walls. Moreover, a plume region outside the discharge channel exit plane is considered in the model. The relative positions of the anode, cathode and magnetic field are consistent with those in the experiment. The secondary electron emission model is considered from the dielectric walls. The mass flow rate m_a=897 μg/s and discharge voltage U_d=200 V are applied at the anode, and 0 V is applied at the cathode.

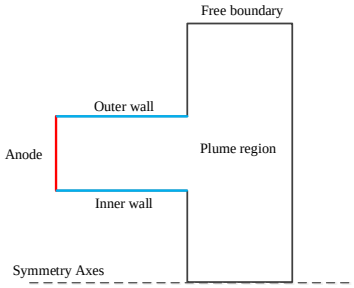

Figure 12. Model of the low power Hall thruster.

The model has made several assumptions, including the Maxwell distribution of the initial particles, quasi-neutral cathode boundary, ignoring the collision of atoms and ions, ignoring the double charge ions, and constant neutral axial velocity. Besides, the model is fully consistent, and the wall energy conservation, anomalous transport (Bohm diffusion), and wall sheaths are considered in the model.

6.2. Parameter analysis

The physical parameter distributions of the ions and atoms inside the discharge channel were mainly considered in the simulation. Figures 13-16 show the number density and axial velocity distributions of Xe and Xe^+. It can be observed from the figures that the ionization principally occur at the center of the discharge channel and the xenon gas near the walls has a lower ionization degree. The ionization region of neutral particles and the acceleration region of the ions are obviously separated, and the maximal ion velocity at the discharge channel exit is more than 15000 m/s, which greatly exceeds that of any unionized particles that may escape from the discharge channel. In addition, the maximal ion number density in the channel exceeds 1×10^{18} m^{-3}. The simulation result of ion velocity is similar with that measured by Wien filter. Therefore, it is proven that our design of the low power Hall thruster has feasibility and rationality.

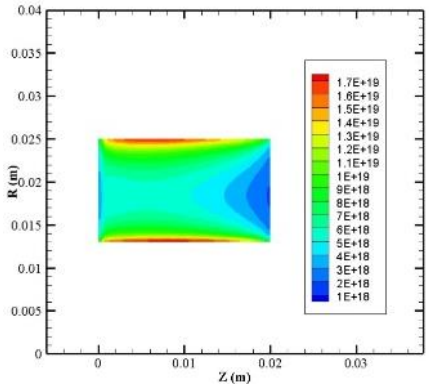

Figure 13. Number density distribution of Xe.

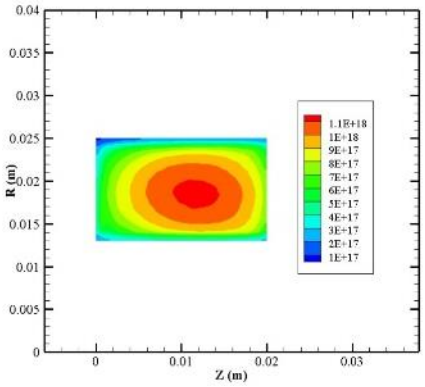

Figure 14. Number density distribution of Xe^+.

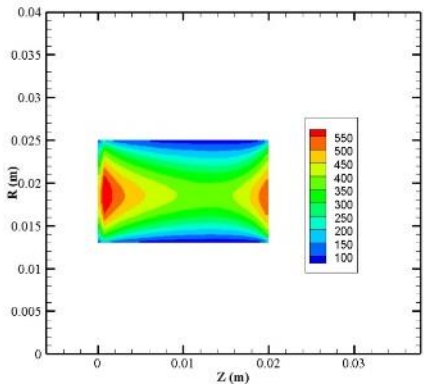

Figure 15. Axial velocity distribution of Xe.

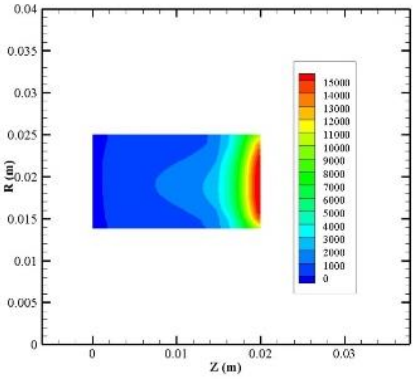

Figure 16. Axial velocity distribution of Xe+.

7. Conclusion

A low power Hall thruster was manufactured, and tested at 200 W-class in the low vacuum electric propulsion experiment platform. During the operation of the thruster, the thrust was directly measured with a thrust target, while the ion current density and the ionic composition and proportion were measured using Faraday probe and Wien filter. At about 200 W of total input power and at a total xenon flow rate of 10.6 sccm, the thrust, anode specific impulse and anode efficiency

are 12.13 mN, 1380 s, and 41.0%, respectively. However, the anode efficiency measured by Wien filter was slightly different from that calculated based on thrust measurement. Moreover, the parameter distributions of Xe and Xe^+ were simulated with PIC method, including number density and axial velocity. The results of simulation indicate the ionization and acceleration regions exist in the midstream and downstream of the discharge channel. The maximal ion velocity is close to that measured in the experiment. A comparison between the experiment and simulation confirms that the designed low power Hall thruster could be suitable for small satellite missions.

References

[1] Bromaghim D et al. 2011, JANNAF Journal of Propulsion and Energetics 4 87-102.

[2] Kim H et al. 2016, Plume and beam properties of a miniaturized low-power (<100W) cylindrical Hall thruster for microsatellites 52nd AIAA/SAE/ASEE Joint Propulsion Conference (Salt Lake City, UT, USA) (Reston, VA: American Institute of Aeronautics and Astronautics) AIAA-2016-5034.

[3] Ikeda T et al. 2011, Research and development of very low power cylindrical Hall thrusters for Nano-Satellites 32nd International Electric Propulsion Conference (Wiesbaden, Germany), IEPC-2011-039.

[4] Ikeda T et al. 2013, Development of Low-Power Cylindrical type Hall Thrusters for Nano Satellite 33rd International Electric Propulsion Conference (Washington, D.C., USA) IEPC-2013-109.

[5] Kakuma T et al. 2015, Research and Development of Low-Power Cylindrical-Type Hall Thrusters for Nano/Micro-Satellites 34th International Electric Propulsion Conference and 6th Nano-Satellites (Hyogo-Kobe, Japan) IEPC-2015-302.

[6] Ikeda T et al. 2012, Research and development of high-efficiency Hall-type ion engines for small spacecrafts Renewable Energy Research and Applications (ICRERA) (Japan).

[7] Frieman J D et al. 2016, Performance evaluation of the T-40 Low-Power Hall current thruster 52nd AIAA/SAE/ASEE Joint Propulsion Conference (Salt Lake City, UT, USA) (Reston, VA: American Institute of Aeronautics and Astronautics) AIAA-2016-4833.

[8] Smimov A et al. 2004, Journal of applied physics 95 2283-2292.

[9] Conversano R W et al. 2017, Performance enhancement of a long-life, low-power hall thruster for deep-space smallsats Aerospace Conference IEEE.

[10] Garrigues L et al. 2019, Plasma Sources Science and Technology 28 034003.

[11] Macdonald-Tenenbaum N et al. 2019, Journal of Propulsion and Power 35 403-412.

[12] Baird M et al. 2021, Applied Sciences 11 1973.

[13] Duan X Y et al. 2020, Plasma Sci. Technol. 22 055501.

[14] Ding Y J et al. 2018, Plasma Sci. Technol. 20 035509.

[15] Szabo J et al. 2012, Journal of Propulsion & Power 28 848-856.